



Editor's Choice

Rovibrational analysis of the water bending vibration in the mid-infrared spectrum of atmospherically significant N₂–H₂O complex



S.D. Springer^a, B.A. McElmurry^a, Z. Wang^a, I.I. Leonov^{a,b}, R.R. Lucchese^a, J.W. Bevan^{a,*}, L.H. Couder^c

^a Department of Chemistry, Texas A&M University, College Station, TX 77843-3255, USA

^b Institute of Apply Physics, Nizhny Novgorod, Russia

^c Laboratoire Inter-Universitaire des Systèmes Atmosphériques, UMR 7583 CNRS et Universites Paris Est Creteil et Paris Diderot, 61, Avenue du General de Gaulle, 94010 Creteil Cedex, France

ARTICLE INFO

Article history:

Received 14 April 2015

In final form 9 May 2015

Available online 10 June 2015

ABSTRACT

Rovibrational transitions associated with tunneling states in the water bending vibration of the atmospherically significant N₂–H₂O complex have been recorded using a cw supersonic jet quantum cascade laser spectrometer at 6.2 μm. Analysis of the observed spectra is facilitated by incorporating fits of previously recorded microwave and submillimeter data. This accounts for Coriolis coupling to obtain the levels of the ground vibrational state and confirmation of assignment of the excited water bending vibration. The results are used to explore the nature of the associated water bending vibrationally excited states of the complex compared to those in other corresponding water complexes.

© 2015 Elsevier B.V. All rights reserved.

1. Introduction

Interaction of water with the major atmospheric species is of considerable significance in chemistry and biochemistry. Formation of N₂–H₂O and O₂–H₂O under atmospheric conditions are especially relevant for the understanding of many chemical and physical phenomena occurring in the Earth's atmosphere. Absorption of light by such complexes can potentially play a significant role in several spectral regions, including the infrared. Spectral shifts, enhancements and broadenings of the absorption lines are expected, suggesting that the dynamics of such weakly interacting systems should be included in the energy balance of the Earth's atmosphere.

The water–nitrogen complex is expected to be one if not the most abundant of water dimer complexes in the Earth's atmosphere with significantly greater abundance than water dimer [1,2]. There has consequently been increased interest in advancing theoretical studies of N₂–H₂O [3,4], particularly with respect to determination of virial coefficients. N₂ collision-induced absorption band intensity arising from interactions between N₂ and H₂O molecules at wavelengths around 4 μm has also been

investigated using the *ab initio* CCSD(T) method complemented by the CBS procedure and FTIR (Fourier transform infrared) laboratory studies [4]. Absorptions due to pure rotational transitions in H₂O occur in the far-IR (<500 cm⁻¹) and are now explicitly accounted for in climate (radiative transfer) models [5]. Although, individual N₂ and O₂ molecules are transparent in the far-IR spectral region, their interactions with water molecules induce low frequency intermolecular modes that can absorb IR radiation giving additional radiation trapping [5]. Microwave spectroscopy has shown that structurally and energetically, the intermolecular bond in the water–nitrogen dimer ground state resembles a weak hydrogen bond [6] with water acting as an electrophile (proton donor). The submillimeter spectrum of the complex has also been observed and reported [7]. Matrix isolation studies have provided infrared spectra, though the determined frequencies are shifted by the presence of matrices [8–10]. Furthermore, there have been FTIR studies of N₂–H₂O and (H₂O)_{n=2–20}–N₂ in the near infrared [11,12]. The spectra of the N₂–H₂O complex in helium nanodroplets have also been recorded in the near-infrared (3700–3900 cm⁻¹) and show two bands separated by about 6 cm⁻¹, that are attributed to the parallel and perpendicular bands of the complex with no internal rotation of H₂O [13]. The harmonic frequencies (and infrared intensities) have been calculated at 70.1(14.2), 81.1(0.01), 91.2(1.7), 181.1(82.6), 269.1(91.6), 1668.0(51.7), 2182.6(0.34), 3872.4(34.3), 3985(149.9) cm⁻¹ [5]. A subsequent calculation

* Corresponding author.

E-mail address: bevan@chem.tamu.edu (J.W. Bevan).

of the equilibrium structure of the dimer agreed with previous predictions of a near linear N–N···H–O–H hydrogen bonded structure and gave an intermolecular bond energy of D_e 441 cm⁻¹ [4.50 kJ mol⁻¹] [14]. Recent papers have reported investigation of this potential using CCSD(T) and aug-ccpVTZ basis sets finding $D_e \sim 280$ cm⁻¹ [15]. A molecular beam scattering study gave a significant different value of only 110 cm⁻¹ [16].

The potential energy surface (PES) of N₂–H₂O away from the minimum of the potential energy surface is not well characterized experimentally. Further studies of the rovibrational manifold associated with intramolecular and intermolecular states are required for a determination of a morphed potential energy surface of the complex and subsequent accurate prediction of dimer properties. Information on the barrier height for interconversion of the two hydrogen/nitrogen atoms in the GS has not been obtained nor has the variation of the barrier height with vibrational states. The multidimensional nature of the tunneling pathways complicates the analysis of the spectra. In the present investigation, a simplified model Hamiltonian has been used in the spectral analysis assuming that the internal rotation of the heavier N₂ subunit leads to a slow J - and K_a -rotational dependence of its tunneling splitting that was ignored [17].

There have been no previously published rovibrational analyses of any fundamental vibrations in the mid- and near infrared spectra range for isolated N₂–H₂O isotopomer. We now report resolved rovibrational transitions including those associated with tunneling in the water bending vibration of the N₂–H₂O complex (ν_2 H₂O monomeric bending vibration) recorded using a quantum cascade laser supersonic jet spectrometer at 6.2 μm. The recorded spectra are expected to show the influence of the tunneling dynamics that involve the exchange of identical sets of hydrogen and/or nitrogen nuclei in the complex. Analysis of the observed spectra is facilitated by incorporating data of previously recorded microwave and submillimeter spectroscopy and accounting for Coriolis coupling to characterize the levels of the ground vibrational state. The results are then used to confirm assignment of the water bending vibration and explore the nature of tunneling dynamics in associated vibrationally excited states of the N₂–H₂O complex.

2. Experimental

All spectra currently reported were recorded using a Quantum Cascade Laser, QCL, (21062-MHF, Daylight Solutions, San Diego, CA, USA) in the water bend region (~1570–1640 cm⁻¹). The laser output frequency is controlled by a combination of coarse and fine tuning of a wavelength selective grating by an internal optical encoder and a piezoelectric actuator or PZT [18]. Application of a voltage in the range of 0–100 VDC to the PZT enables mode-hop-free coverage of approximately 1.7 cm⁻¹ with an effective instrumental resolution of 0.001 cm⁻¹. The laser output was split using CaF₂ windows and directed through appropriate optics to the supersonic slit expansion, a Fabry-Pérot confocal etalon (Spectra-Physics, SP5945, FSR of 0.006962456 cm⁻¹) for relative frequency calibration, and a reference cell containing NO₂ and H₂O for absolute frequency calibration. Such measurements were used for calibration of absolute frequencies to an accuracy of ±0.0005 cm⁻¹ in the current studies. All spectra were recorded using wavelength modulation spectroscopy and second derivative lock-in detection.

Argon carrier gas was bubbled through a custom-made water sparger (50 mm diameter, 1 m length) and combined with nitrogen gas in a premixing manifold. The continuous supersonic expansion was generated through a 12 cm long by 25 μm wide slit, into a vacuum chamber with a pressure of 700 mTorr pumped by a Leybold RA2001 Roots blower and backed by Leybold SV630F roughing pump. The expansion was probed by a portion of the laser radiation

Table 1
Hamiltonian matrix elements for N₂–H₂O.

Symmetry species	Matrix elements	Statistical weight
Rotational ^a	Overall ^b	
A'	A_1^+	$H_{JK1;JK1} + H_{JK1;JK3} + H_{JK1;JK4}$
A'	B_1^+	$H_{JK1;JK1} - H_{JK1;JK3} + H_{JK1;JK4}$
A'	B_2^+	$H_{JK1;JK1} - H_{JK1;JK3} - H_{JK1;JK4}$
A'	A_2^+	$H_{JK1;JK1} + H_{JK1;JK3} - H_{JK1;JK4}$
A''	A_1^-	$H_{JK1;JK1} + H_{JK1;JK3} + H_{JK1;JK4}$
A''	B_1^-	$H_{JK1;JK1} - H_{JK1;JK3} + H_{JK1;JK4}$
A''	B_2^-	$H_{JK1;JK1} - H_{JK1;JK3} - H_{JK1;JK4}$
A''	A_2^-	$H_{JK1;JK1} + H_{JK1;JK3} - H_{JK1;JK4}$

^a The symmetry species of the rotational function in C_S is given in this column.

^b The symmetry species in G_8 of the rotation-tunneling wavefunction is given in this column.

at approximately 2 mm from the exit of the slit and optimized for the largest observed signal. Due to the nature of the introduction of water, it was not possible to directly account for the relative concentration of water in the expanding gas; however it is estimated to constitute around 0.5–1.0%. Therefore the expansion gas was composed of 1% H₂O, 7% N₂ and 92% at a pressure of 1–2 bar.

A total of 265 infrared rovibrational transitions belonging to the $K=0 \leftarrow 0$, $1 \leftarrow 0$ and $0 \leftarrow 1$ bands were observed and assigned in the 6.2 μm region. As emphasized by Figure 2, nitrogen tunneling states were resolved for the $K=1 \leftarrow 0$ band. They were also resolved for the $K=0 \leftarrow 1$ band but not for the $K=0 \leftarrow 0$ band due to our limitations in instrumental resolution. Current data was compiled along with available microwave and submillimeter data from previous studies to account for a total of 306 infrared and 123 microwave and submillimeter transitions [6,7] in two separate fits (Supplementary Materials) with 41 unresolved $K=0 \leftarrow 0$ infrared transitions in both fits.

3. Spectroscopic analysis

The energy level diagram of the non-rigid N₂–H₂O dimer in its ground vibrational state has been derived by Leung et al. [6] and is drawn in their Fig. 6. Their results can also be used in the case of the excited vibrational state observed in this work as this state is a symmetrical one with the water molecule having one quantum of energy in its symmetrical bending ν_2 mode. As emphasized by Fig. 6 of Leung et al. [6], the rotational levels are split into four tunneling sublevels due to two large amplitude tunneling motions. The large and small splittings originate from the large amplitude motions corresponding to internal rotations of the lighter water subunit and of the heavier N₂ subunit, respectively. The symmetry group to be used for N₂–H₂O is the commutative group introduced in Section 7B of Coudert and Hougen [19] for the D₂O–H₂O dimer. This group will be denoted G_8 and its character table can be found in Tables VIII of this reference.

The approach used to calculate the rotation-tunneling energies in this work makes use of the results of Coudert and Hougen [19,20] and of the atom and framework numbering of Leung et al. [6] given in their Fig. 5. The most feasible large amplitude motion, corresponding to a planar internal rotation of the water subunit, allows us to go from framework 1 to framework 3 and will be named the $1 \Rightarrow 3$ tunneling motion. The less feasible large amplitude motion, corresponding to the internal rotation of the N₂ subunit, allows us to connect frameworks 1 and 4 and will be named the $1 \Rightarrow 4$ tunneling motion. The expressions of the Hamiltonian matrix elements are given in Table 1 for each symmetry species of G_8 . In addition to the matrix element of the rotational Hamiltonian $H_{JK1;JK1}$, these expressions involve the tunneling matrix elements $H_{JK1;JK3}$ and $H_{JK1;JK4}$. The former should be obtained from Eq. (33) of Coudert and Hougen [19] where θ_2 and h_{2v} should be changed into

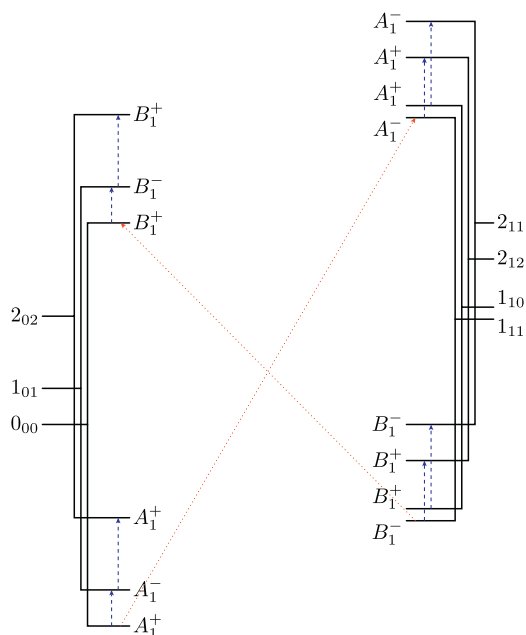


Figure 1. Simplified energy level diagram for the $\text{N}_2\text{-H}_2\text{O}$ dimer. Only tunneling sublevels with $J \leq 2$ and $K_a \leq 1$ appear in this figure. Vertical dashed (oblique dotted) lines indicate a few a -type (b -type) transitions. The large tunneling splitting is due to the large amplitude motion involving a planar rotation of the water moiety. A similar diagram arises for tunneling sublevels belonging to the A_2^\pm and B_2^\pm symmetry species.

θ_3 and h_{3v} , respectively; the latter should also be obtained from these equations changing θ_2 and h_{2v} into θ_4 and h_{4v} , respectively, and removing the $(-1)^K$ factor. Parameters h_{3v} and h_{4v} are both negative [3] and are such that $2|h_{3v}|$ and $2|h_{4v}|$ are the tunneling splittings associated with the $1 \rightarrow 3$ and $1 \rightarrow 4$ tunneling motions for $J=0$, respectively. Due to the fact that the $1 \rightarrow 3$ large amplitude motion is more feasible than the $1 \rightarrow 4$, we also have $h_{3v} < h_{4v} < 0$. Parameters θ_3 and θ_4 describe the rotational dependence of the tunneling splittings and are expected to be on the order of a few degrees.

The rotation-tunneling energy of $\text{N}_2\text{-H}_2\text{O}$ should be calculated setting up with the help of Table 1 and diagonalizing the matrices arising for each symmetry species of G_8 . The resulting energies depend on the usual rotational constants A , B , C and on the tunneling parameters θ_3 , h_{3v} , θ_4 , h_{4v} . Two such sets of parameters are needed in the present investigation. The first one corresponds to the ground vibrational state; the second one to the excited vibrational state with the water molecule in its excited (010) vibrational state. In order to parameterize the energy difference between these two vibrational states and additional parameter arises and will be denoted C_0 .

The rotation-tunneling energy level diagram can be simplified because the effects of the $1 \rightarrow 4$ tunneling motion can be ignored as (i) it being not very feasible the associated tunneling splitting is small and (ii) selection rules require that transitions connect the two lower or the two upper tunneling sublevels which prevents us from observing directly the tunneling splitting. Two independent energy level diagrams can thus be used and are characterized by different rotational constants and h_{3v} and θ_3 values. As can be inferred from Table 1, the first diagram involves levels of A_1^\pm and B_1^\pm symmetry species belonging to the lower tunneling sublevel of the $1 \rightarrow 4$ tunneling motion; the second one involves levels of A_2^\pm and B_2^\pm symmetry species belonging to the upper tunneling sublevel. The simplified energy level diagram arising when making the former assumption is shown in Figure 1. These results are also

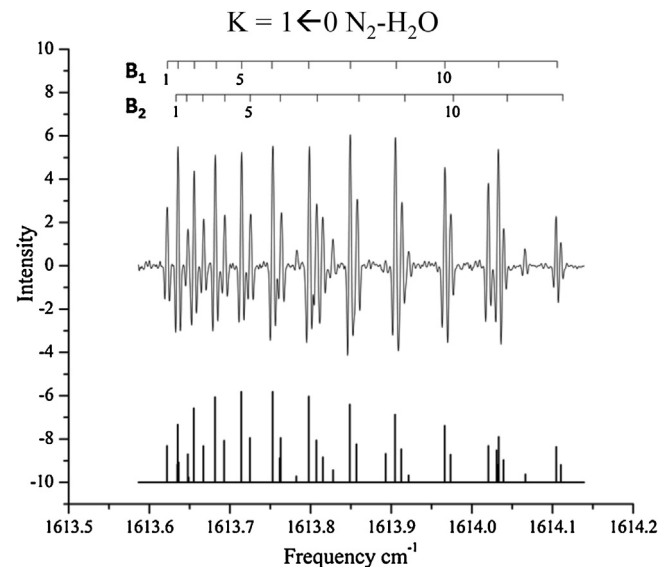


Figure 2. A small portion of the infrared spectrum recorded in this work for $\text{N}_2\text{-H}_2\text{O}$ dimer. The Q branch of one of the b -type bands can be seen. Transitions display a small splitting due to the large amplitude motion corresponding to the internal rotation of the N_2 moiety of the dimer.

valid for the excited vibrational state of the dimer observed in this work.

4. Line assignment and analysis

The infrared transitions recorded in this work were assigned with the help of the statistical weights in Table 1. a -Type transitions with $K=0$ connecting the ground state to the excited vibrational state and involving all four types of tunneling sublevels were observed. These transitions displayed no splitting due to the $1 \rightarrow 4$ tunneling motion which results in unresolved A_1^\pm and A_2^\pm or the B_1^\pm and B_2^\pm tunneling components. The effects of the $1 \rightarrow 3$ tunneling motion were, however, observed as they lead to a 0.2 cm^{-1} splitting increasing J . $K=1 \leftarrow 0$ and $0 \leftarrow 1$, b -type transitions were also observed and were split into four components. The large splitting on the order of 2 cm^{-1} originates from the $1 \rightarrow 3$ tunneling motion; the small one on the order of 0.01 cm^{-1} stems for the change of the $1 \rightarrow 4$ tunneling splitting when going from $K=0$ to $K=1$. This small splitting can be seen in Figure 2 where the Q branch of one of the b -type bands can be seen.

A line position analysis of the infrared data recorded in the present investigation (Supplementary Materials) and of previous microwave data pertaining to the ground vibrational [6,7] was performed in which the energy was calculated as outlined in the previous section. Two analyzes were performed treating separately transitions involving A_1^\pm and B_1^\pm sublevels and those involving A_2^\pm and B_2^\pm sublevels. The parameters determined in the fit are listed in Table 2. Distortion terms for the pure rotational Hamiltonian were expressed using Watson's S reduction [21]. Distortion effects for the tunneling terms were accounted for using the same operators as Coudert and Hougen [19].

5. Discussion

The current rovibrational analysis of the water bending vibration in $\text{N}_2\text{-H}_2\text{O}$ provides a stark contrast with that of the corresponding water dimer [22]. The bending vibrations of H_2O dimer have been investigated by cavity ring down spectroscopy with a resolution of 0.04 cm^{-1} . Blue shifted bands have been recorded at 1600.6 , 1613.8 , 1614.7 cm^{-1} and 1628.6 cm^{-1} . The

Table 2Parameters^a determined in the line position analysis.

	Ground		Excited	
	A_1^\pm/B_1^\pm	A_2^\pm/B_2^\pm	A_1^\pm/B_1^\pm	A_2^\pm/B_2^\pm
C_0				1597.00072(21)
A	17.044818(3)	17.026097(1)	17.62043(38)	17.59433(34)
B	0.09782208(21)	0.09772371(18)	0.0981953(97)	0.098123(16)
C	0.0963608(130)	0.09644802(18)	0.0965892(90)	0.096631(15)
$D_{KJ}/10^{-3}$	-2.4315(37)	-2.57378(11)	-3.023(13)	-3.183(12)
$D_{JJ}/10^{-6}$	1.4199(61)	1.3881(19)	1.561(48)	1.493(37)
$d_1/10^{-6}$	0.2829(29)	0.1125(26)		0.167(65)
$H_{KJ}/10^{-6}$	-0.7202(63)	-1.1356(23)	-0.9744(890)	-1.057(91)
$H_{JJ}/10^{-9}$	0.111(17)	-0.0602(130)		
$h_1/10^{-9}$	-0.301(23)	-0.3455(210)		
h_{3v}	-0.531609(21)	-0.51810688(59)	-0.33848(23)	-0.32470(21)
θ_3	1.591(330)	1.882(390)	1.591 ^b	1.882 ^b
h_{3k}			-0.04400(31)	-0.03291(30)
$h_{3j}/10^{-3}$	-0.2232(430)	-0.271802(46)	-0.1704(70)	-0.209(34)
$f_{3j}/10^{-3}$	0.1786(220)	0.141059(77)	0.1490(29)	0.1066(25)
$h_{3kj}/10^{-3}$	-0.17433(29)	-0.35408(14)	-0.0963(47)	-0.2822(91)
$h_{3jj}/10^{-7}$	-0.925(390)	-0.086(16)	-1.28(43)	-1.209(74)
$f_{3j}/10^{-7}$	-0.249(380)	2.463(20)		
$h_{3kj}/10^{-6}$	-0.2150(180)	0.2375(26)		
$h_{3jj}/10^{-10}$	0.373(320)	-1.10(12)		

^a Parameters are in cm^{-1} except θ_3 which is in degrees. Uncertainties are given in parentheses in the same units as the last digit.^b Parameter θ_3 was constrained to be equal for the ground and excited vibrational states.

first band is associated with a perpendicular acceptor band with $\Delta K=0$ while the others are $\Delta K=1$ involving the donor water bend. The pre-dissociative lifetime of states in H_2O dimer is significantly shorter than in $\text{N}_2-\text{H}_2\text{O}$. Recently, the dissociation energy of H_2O dimer [23] has been determined experimentally to be $1105(10)\text{ cm}^{-1}$. Based on the Ewing's propensity rules [24] and trajectories leading to dissociation in water dimer have been discussed [25] and are compatible with the observed spectral bands. The dissociation energy of $\text{N}_2-\text{H}_2\text{O}$ has not been experimentally determined though it is expected to be approximately half that of $\text{OC}-\text{H}_2\text{O}$. The latter is known [26] to have $D_0=355(13)\text{ cm}^{-1}$ with well resolved rovibrational substructure [27] in its bending vibration, so it is expected that the predissociative line broadening should be significantly less than that in H_2O dimer which is what is observed for $\text{N}_2-\text{H}_2\text{O}$ in Figure 2. The current rovibrational analysis is valuable for generation of accurate rovibrational spectroscopic data for the potential energy surface of $\text{N}_2-\text{H}_2\text{O}$ and assessing of quantum chemical calculations used to evaluate intensities of vibrations as a function of temperature on the quantitation of $\text{N}_2-\text{H}_2\text{O}$ continuum [4]. These results are also now available for comparison with the corresponding ν_2 bending vibration in the recorded spectrum [28] of $\text{N}_2-\text{D}_2\text{O}$.

As emphasized by Table 2, more distortion parameters were used for the ground vibrational state than for the excited one. This stems from fact that the data set contains accurate microwave data only for the ground state. In order to reproduce the wavenumber of the infrared lines within 0.001 cm^{-1} , we were led to vary for the excited vibrational state an h_{3k} distortion parameter describing $1 \rightarrow 3$ tunneling motion effects. A few poorly determined distortion parameters in the pure rotational Hamiltonian had also to be varied. The angle θ_3 can be related to the angle through which the water subunit is rotated [19] during the $1 \rightarrow 3$ tunneling motion. Taking a value of 9.524 cm^{-1} for the C rotational constant of the water subunit, the angle values retrieved are 157° and 186° for the A_1^\pm/B_1^\pm and A_2^\pm/B_2^\pm levels, respectively. Chemical intuition suggests that this angle should be close to the valence angle of the water subunit, 104.5° . The agreement is very poor and this might be due to the N_2 and water units being much closer for the intermediate configuration of the $1 \rightarrow 3$ large amplitude motion than for the equilibrium configuration. The θ_3 value retrieved in the analysis may also be contaminated by distortion

effects due to the limited range of K -values available in the data set.

In addition, the current analysis has relevance to the interpretation of the doublet [29] assigned to the 0.15 cm^{-1} resolution 1593 cm^{-1} $\text{N}_2-\text{H}_2\text{O}$ spectrum of water trapped in solid argon doped with nitrogen that was complicated by overlap with the simultaneously recorded spectrum of water dimer.

6. Conclusions

The rovibrationally resolved spectrum of the water bending vibration in $\text{N}_2-\text{H}_2\text{O}$ has been recorded. This spectrum has been analyzed from the perspective of large and small splittings originating from the large amplitude motions corresponding to internal rotations of the lighter water subunit and of the heavier N_2 subunit, respectively. The results confirm that predissociative line broadening in the bending vibration of this atmospherically significant complex is fundamentally different from that in the less abundant water dimer. This spectroscopic analysis contributes accurate spectroscopic data toward a comprehensive characterization of the potential energy function of the complex and its relevance in atmospheric chemistry.

Acknowledgements

We express special thanks to the Robert A Welch Foundation (Grant A747) for financial support in the form of a post-doctoral fellowship for Blake A. McElmurry and a pre-doctoral fellowship for Sean D. Springer. In addition, we also wish to thank LST/STTAMU for supporting this research.

Appendix A. Supplementary data

Supplementary data associated with this article can be found, in the online version, at doi:10.1016/j.cplett.2015.05.050

References

- [1] V. Vaida, J. Chem. Phys. 135 (2011) 020901.
- [2] J.S. Daniel, S. Solomon, H.G. Kjaergaard, D.P. Schofield, Geophys. Res. Lett. 31 (2004) L06118.

- [3] A.A. Vigasin, Z. Slanina, *Molecular Complexes in Earth's Planetary, Cometary and Interstellar Atmospheres*, World Scientific, Singapore, 1998.
- [4] Y.I. Baranov, I.A. Buryak, S.E. Lokshtanov, V.A. Lukyanenko, A.A. Vigasin, *Phil. Trans. R. Soc. A* 370 (2012) 2691.
- [5] I.M. Svirshchev, R.J. Boyd, *J. Phys. Chem. A* 102 (1998) 7294.
- [6] H.O. Leung, M.D. Marshall, R.D. Suenram, F.J. Lovas, *J. Chem. Phys.* 90 (1989) 700.
- [7] P.A. Stockman, *Microwave and Far Infrared Spectroscopy of Water-Containing, Hydrogen-Bonded Dimers: Vibrational Rotational, and Tunneling Dynamics* (Ph.D. dissertation), California Institute of Technology, 1995.
- [8] L. Andrews, S.R. Davis, *J. Chem. Phys.* 83 (1985) 4983.
- [9] A. Engdahl, B.J. Nelander, *Mol. Struct.* 193 (1989) 101.
- [10] S. Coussan, A. Loutellier, J.P. Perchard, S. Racine, S.Y.J. Bouteiller, *Mol. Struct.* 471 (1998) 37.
- [11] J. Sadlej, B. Rowland, J.P. Devlin, V. Buch, *J. Chem. Phys.* 102 (1995) 4804.
- [12] W. Hujo, M. Gaus, M. Schultze, T. Kubar, J. Grunenberg, M. Elstner, S. Bauerecker, *J. Phys. Chem. A* 115 (2011) 6218.
- [13] S. Kuma, M.N. Slipchenko, K.E. Kuyanov, T. Momose, A.F. Vilesov, *J. Phys. Chem. A* 110 (2006) 10046.
- [14] A.S. Tulegenov, R.J. Wheatley, M.P. Hodges, A.H. Harvey, *J. Chem. Phys.* 126 (2007) 094305.
- [15] P.R.B. Barreto, A.F. Albernaz, A. Capobianco, F. Palazzetti, A. Lombardi, G. Grossi, V. Aquilanti, *Comput. Theor. Chem.* 990 (2012) 53.
- [16] D. Cappelletti, P. Candori, L.F. Roncaratti, F. Pirani, *Mol. Phys.* 108 (2010) 2179.
- [17] R.E. Bumgarner, S. Suzuki, P. Stockman, P.A. Green, P.G.G.A. Blake, *Chem. Phys. Lett.* 176 (1991) 123.
- [18] B.A. McElmurry, L.A. Rivera-Rivera, K.W. Scott, Z. Wang, I.I. Leonov, R.R. Lucchese, J.W. Bevan, *Chem. Phys.* 409 (2012) 1.
- [19] L.H. Coudert, J.T. Hougen, *J. Mol. Spectrosc.* 130 (1988) 86.
- [20] L.H. Coudert, F.J. Lovas, R.D. Suenram, J.T. Hougen, *J. Chem. Phys.* 87 (1987) 6290.
- [21] J.K.G. Watson, in: J.R. Durig (Ed.), *Vibrational Spectra and Structure*, vol. 6, Elsevier, Amsterdam, 1977, p. 1.
- [22] J.B. Paul, R.A. Provencal, C. Chapco, K. Roth, R. Caseas, R.J. Saykally, *J. Phys. Chem. A* 103 (1999) 2972.
- [23] B.E. Rocher-Casterline, L.C. Ch'ng, A.K. Mollner, H. Reisler, *J. Chem. Phys.* 134 (2011) 211101.
- [24] G.E. Ewing, *J. Phys. Chem.* 91 (1987) 4662.
- [25] A.K. Samanta, G. Czako, Y. Wang, J.S. Mancini, J.M. Bowman, H. Reisler, *Acc. Chem. Res.* 47 (2014) 2700.
- [26] L.A. Rivera-Rivera, B.A. McElmurry, K.W. Scott, R.R. Lucchese, J.W. Bevan, *J. Phys. Chem. A* 117 (2013) 8477.
- [27] L.A. Rivera, L.A. Springer, S.D. McElmurry, B.A. Wang, Z. Leonov, I.I. Lucchese, R.R. Bevan, J.W. L.H. Coudert, Unpublished results.
- [28] Y. Zhu, R. Zhengm, S. Li, C. Duan, *J. Chem. Phys.* 139 (2013) 214309.
- [29] C. Pardanaud, C. Vasserot, A.-M. Michaut, X.L.J. Abouaf-Marginu, *Mol. Struct.* 873 (2008) 181.